Differences of Regulative Flexibility between Hydrological Isolated and Connected Lakes in a Large Floodplain: Insight from Inundation Dynamics and Landscape Heterogeneity

Jiakun Teng [1,2], **Shaoxia Xia** [1,*], **Yu Liu** [1], **Peng Cui** [3,4,5], **Jiang Chen** [6], **Wuwei Si** [7], **Houlang Duan** [1,2] **and Xiubo Yu** [1,2,*]

[1] Key Laboratory of Ecosystem Network Observation and Modeling, Institute of Geographic Sciences and Natural Resources Research, Chinese Academy of Sciences, Beijing 100101, China; jiakunteng@163.com (J.T.); liuyu@igsnrr.ac.cn (Y.L.); duanhl2408@126.com (H.D.)

[2] College of Resources and Environment, University of Chinese Academy of Sciences, Beijing 100101, China

[3] Research Center for Nature Conservation and Biodiversity, Nanjing Institute of Environmental Sciences, Ministry of Ecology and Environment, Nanjing 210042, China; cuipeng1126@163.com

[4] State Environmental Protection Scientific Observation and Research Station for Ecological Environment of Wuyi Mountains /Biodiversity Comprehensive Observation Station for Wuyi Mountains, Nanjing 210042, China

[5] State Environmental Protection Key Laboratory on Biosafety, Nanjing 210042, China

[6] Office of Poyang lake water control project construction of Jiangxi Province, Nanchang 330009, China; chhb5181@163.com

[7] Poyang Lake hydrological bureau in Jiangxi, Jiujiang 332800, China; pyhzh@163.com

* Correspondence: xiasx@igsnrr.ac.cn (S.X.); yuxb@igsnrr.ac.cn (X.Y.); Tel.: +86-6488-9820 (X.Y.)

Abstract: The inundation areas of floodplains are crucial to wetland ecosystems, especially in supporting biodiversity. Accurately identifying the spatial and temporal patterns of inundation areas is important for understanding floodplain ecosystem processes. Here, lakes in the Yangtze River Floodplain were divided into two types according to hydrological conditions: the natural connected lakes (Dongting Lake and Poyang Lake) with natural water level fluctuations and the isolated lakes (lakes in Jianghan Plain) with stable water levels. We established a method to identify inundation areas using multi-sources remote sensing data based on the Google Earth Engine. The dynamics of inundation areas were determined, and the relative indices were calculated in common year (2017) and a drought year (2018). The differences between the connected lakes and the isolated lakes were analyzed, and impacts of hydrological fluctuations on inundation area and habitat quality were evaluated. The results show that lakes with natural hydrological fluctuations have a greater regulative flexibility, with both patch density (PD) and submerged elasticity index (SEI) values higher than that of isolated lakes. The trend of the vegetation index in the connected lakes and in the isolated lakes is also different. The mean EVI in Dongting Lake and Poyang Lake showed a U-shaped trend which is similar to the shape of the trend of PD. The trend of mean enhanced vegetation index (EVI) in the isolated lakes is the opposite and has a lower range of variation over a year. This study provides new indicators and rapid methods for habitat quality assessment in floodplains, as well as presenting scientific information useful for improving wetland management in the middle and lower Yangtze River.

Keywords: inundation area; hydrological connectivity; remote sensing images; Google Earth Engine; Yangtze River Floodplain

1. Introduction

Floodplains are among the most productive ecosystems in the world and the inundation area, in particular, is an important component which is critical to biodiversity conservation [1,2]. Most fundamental ecological functions and services in the floodplain ecosystem, such as flood mitigation, food production, recreation and biodiversity sustenance, and the support of human wellbeing and cultural values, are related to the inundation area [3]. In the wet season in the floodplain basin, monsoonal rains lead to gradually rising water levels which deliver sediment and nutrients to the inundation areas [4], while, in the dry season, the water level drops, exposing inundation wetlands provide sustenance for many creatures, and triggering important life cycle processes [5]. Hydrological factors are the core driving force to maintain ecological process and function in wetland ecosystems [6]. Dynamics of flood duration, the timing of exposed and submerged that caused by water level fluctuations, are key factors that shaped differences in wetland landscapes [7]. Therefore, identifying the spatiotemporal pattern of inundation areas is important for figuring out wetland changes and their processes. The Yangtze River is a typical large floodplain [8], however inundation areas in this region have decreased dramatically due to the building of dams and reclamation of land for agriculture [9]. Loss of inundation areas might lead to changes in wetland landscape structure and a decline of biological habitat and biodiversity [10,11].

Figuring out the spatial and temporal pattern of inundation areas accurately and timely is important for revealing the ecosystem processes of floodplains [12]. The inundation area is an important parameter in hydrodynamic modelling. In fact, it was assumed that static variables were represented due to a lack of data and inefficient extraction methods, which affect simulation accuracy [13,14] due to the limited the understanding of the internal feedback mechanisms for hydrological models and hydrodynamics [15]. The recent open assess time series remote sensing data enables the effective extraction of information on large-scale water surfaces, which can be used to identify inundation areas and their dynamics [16,17].

However, existing extraction methods based on remote sensing information, such as visual interpretation and object-oriented extraction, are inefficient. The spatiotemporal patterns of inundation areas in the floodplain are highly dynamic due to hydrological change [18]. Most of the studies above used specific satellite imageries or one composite image from a specific stage when mapping inundation areas, which cannot capture these rapid changes [19,20]. Therefore, to present the status and dynamics of inundation areas accurately, time-series satellite images with medium and high temporal resolution are required. These images require a large amount of data interpretation and analysis work, which leads to challenges in terms of data computation and storage [21]. The development of cloud-based computing power, such as the Google Earth Engine (GEE), has created a great potential for processing large-scale remote sensing data. GEE provides researchers with a large amount of multi-sourced remote sensing data, including Landsat, Modis, Sentinel, and related data products, as well as online parallel computing capabilities for high-performance cloud computing [22]. Recently, cloud computing based on GEE platforms has effectively supported global intertidal extraction [23,24], forest identification [22,25], the extraction of rice growing areas [26,27], and open water body determination [23,28,29].

Inundation areas are the dominant component in the middle and lower Yangtze River floodplain, which support the functioning of the whole ecosystem, as well as biodiversity, through material and energy exchange driven by wet-dry alternation [5]. These areas are also critical for long-distance migratory water birds along the East Asia and Australian Flyway [30]. Most of these migratory birds depend on inundation areas as their wintering habitat [31]. Over the past several decades, in 1950s–1970s in particular, most lakes in this region have been cut off from the natural rhythms of the Yangtze River through the construction and operation of a series of dams or sluice gates, leaving only Dongting Lake and Poyang Lake which have naturally hydrological connectivity in the river basin. Whether there are differences between naturally connected lakes and the hydrologically isolated lakes physically? In particular, do the connected lakes have better flexibility than the isolated ones? To answer this question, it is necessary to extract the inundation areas as quickly as possible and make a quantitative analysis. Here, we establish the method to identify

inundation areas of lakes from the multi-source remote sensing database on GEE, quantitatively analyze the structure and the dynamics of connected and isolated lakes by using the patch density (PD) and the submerged elasticity index (SEI, submerged elasticity index) in a common year (2017) and a drought year (2018).

Our study presents an effective method and the thresholds to determine inundation areas, which makes the identification of such areas rapidly and accurately. Compared with the original visual interpretation, it improves the efficiency of data processing. This study also constructs a time series of inundation areas based on multi-sources remote sensing data and established a quantitative indicator (SEI) to evaluate the lakes' regulative flexibility. The results can provide important scientific information for habitat management and conservation in floodplain areas.

2. Materials and Methods

2.1. Study Area

The middle and lower Yangtze River basin are affected by a typical subtropical monsoon climate. The average annual precipitation is between 1000 and 1400 millimeters, which deposited into the basin mainly in April to July, accounting for approximately 42% to 53% of the annual rainfall, while during the November to next February, the average annual precipitation is very little [32]. The unbalanced seasonal distribution of rainfall leads to changes in wetland areas. Take Poyang Lake for example, its water level difference between dry and wet season is nearly 14 m [33], which leads to the significant differences of lake areas in dry (only about 146 km^2) season and wet (almost 4070 km^2) season [34]. The annual average temperature is 18 °C, and the average winter temperature is about 5 °C. The freshwater lakes in the Yangtze River basin include Dongting Lake (DT) in Hunan province (Figure 1a) and Poyang Lake (PY) in Jiangxi province (Figure 1c), which are connected to the Yangtze River and have a seasonal wet-dry cycle [3]. Intra-annual water level fluctuations form inundation areas, which are critical for the habitats of water birds and other wild animals.

Additionally, there are some lakes now isolated from the Yangtze River due to reclamation for agricultural and rural development, as well as hydrological facilities. For example, the Jianghan Plain in Hubei province (Figure 1b) used to have 1066 lakes, but some of them were cut off from the Yangtze River by dams and sluices. In this study we choose the two connected lakes and nine isolated lakes in Jianghan Plain with areas of more than 3000 Ha. The nine isolated lakes are: (1) Zhangdu Lake; (2) Dong Lake; (3) Tangxun Lake; (4) Niushan Lake; (5) Lu Lake; (6) Futou Lake; (7) Baoan Lake; (8) Liangzi Lake; and (9) Xiliang Lake.
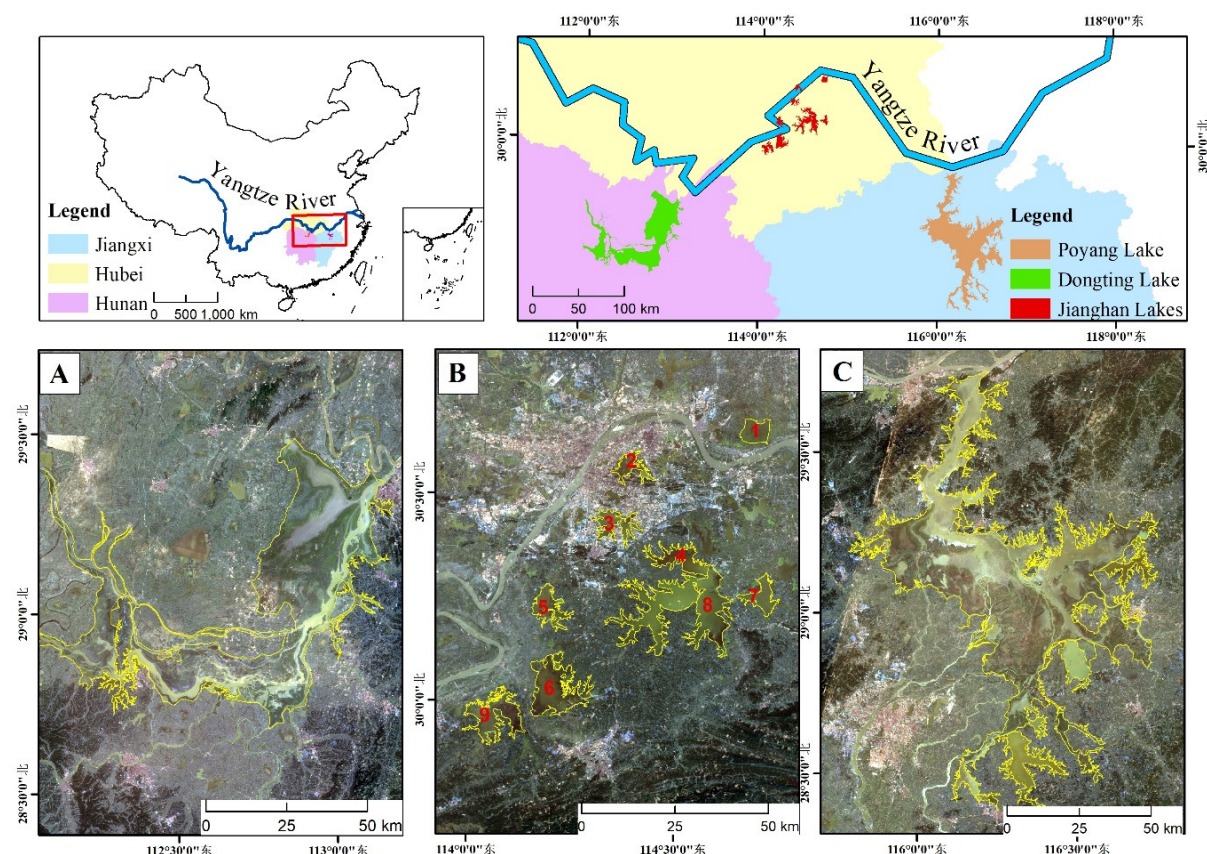
Figure 1. Location of the study area: (**A**). Dongting Lake (DT). (**B**). Jianghan Lakes (JH), which consists of (1) Zhangdu Lake; (2) Dong Lake; (3) Tangxun Lake; (4) Niushan Lake; (5) Lu Lake; (6) Futou Lake; (7) Baoan Lake; (8) Liangzi Lake; and (9) Xiliang Lake. (**C**). Poyang Lake (PY). The satellite image of the study area is the median value of Sentinel-2 in 2018, which uses the color composite of the Sentinel-2 time-series: blue = band 2, green = band 3, and red = band 4.

2.2. Satellite Data Acquisition and Pre-Processing

Satellite data derived from Sentinel-2 images and Landsat Operational Land Imager (OLI) images. The spatial resolutions of Sentinel-2 and Landsat OLI are 10 m and 30 m, respectively. In this paper, all images are resampled to 30 m resolution for analysis in GEE. To ensure that we had a high quality image dataset, the image selection used two criteria: (1) the image must be complete, to ensure it contains the same analysis unit; (2) the cloud area must be less than 30%, to reduce the influence of cloud on the accuracy of the extraction results. Following these criteria, incomplete images and images with a high proportion of cloud were removed. Satellite images from 2017 and 2018 were used to make the comparative analysis. In total, more than 1000 images were used in this study.

We select the same spectral bands from the two sets of data, i.e., red, green, blue, near-infrared spectra, and short-wave infrared which correspond to bands B2, B3, B4, B8, and B6 in the Sentinel-2 images, and B2, B3, B4, B5, and B11 in the Landsat OLI images. The target images were archived in GEE as an image collection and subsequently processed in GEE following the workflow shown in Figure 2. All the images were geometrically rectified and pixel values were converted into surface reflectance.
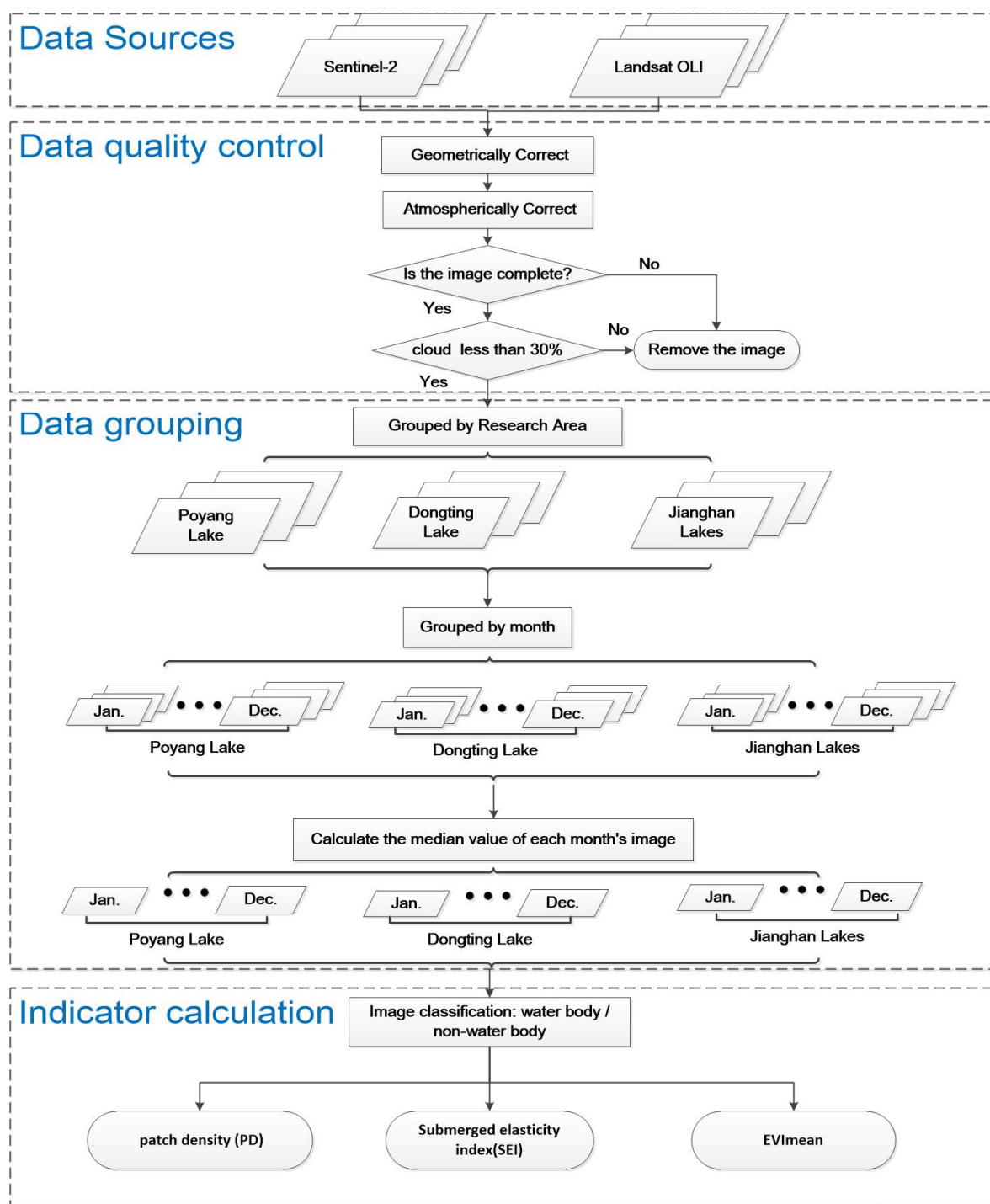
Figure 2. Workflow of the data processing of Sentinel-2 and Landsat Operational Land Imager (OLI) time-series images in the Google Earth Engine (GEE) platform.

2.3. Data Grouping

To analyze the differences between lakes, the image collection was classified by the lake boundaries and divided into three collections: DT, PY, and JH. Each lake boundary was determined visually, checked against Google Earth images, and used as masks to exclude redundant terrestrial areas. Images for each lake were grouped by month and those collections in 2017 and in 2018 were obtained to represent the dynamics of the lake within each of the years under study. In order to balance the influence of low-quality images and obtain the full picture of a specific month, we used the median value of each pixel in the same month to represent the average hydrological situation of the month. Multi-source data were collected to ensure, as far as possible, that the available images

covered both the dry and wet periods of each lake. There were at least eight available images for each lake for each year, which enabled us to determine the variation of each lake's inundation area (Table 1).

Table 1. Remote sensing data source for DT, PY, and JH in 2017 and 2018.

| | 2017 | | | 2018 | | |
Month	**DT**	**PY**	**JH**	**DT**	**PY**	**JH**
January	——	——	Sentinel-2	——	Sentinel-2	——
February	Sentinel-2	Sentinel-2	Landsat OLI	Sentinel-2	Sentinel-2	Landsat OLI
March	——	——	——	Sentinel-2	Sentinel-2	Sentinel-2
April	Landsat OLI	Sentinel-2	Sentinel-2	Sentinel-2	Sentinel-2	Sentinel-2
May	Sentinel-2	Landsat OLI	Sentinel-2	——	——	——
June	Landsat OLI	——	——	Landsat OLI	Sentinel-2	Landsat OLI
July	Sentinel-2	Sentinel-2	Sentinel-2	Sentinel-2	Sentinel-2	Sentinel-2
August	Sentinel-2	Sentinel-2	Sentinel-2	Sentinel-2	Sentinel-2	Sentinel-2
September	Sentinel-2	Sentinel-2	Sentinel-2	——	Sentinel-2	Sentinel-2
October	Sentinel-2	Sentinel-2	Sentinel-2	Sentinel-2	Sentinel-2	Sentinel-2
November	Sentinel-2	Sentinel-2	Sentinel-2	Sentinel-2	Sentinel-2	Sentinel-2
December	——	Sentinel-2	Sentinel-2	——	——	Sentinel-2

2.4. Indicator Calculation

2.4.1. Algorithms to Extract Water Bodies

Modified normalized difference water index (mNDWI), a widely used water-related spectral index, was calculated from satellite data on the GEE platform. mNDWI is sensitive to open surface water bodies. Two vegetation indices related to vegetation greenness: Nominalized difference vegetation index (NDVI) and enhanced vegetation index (EVI) were also calculated. Together, these indices have been used to identify open surface water bodies [18],

$$mNDWI = \frac{\rho_{green} - \rho_{swir}}{\rho_{green} + \rho_{swir}} \tag{1}$$

$$EVI = 2.5 \times \frac{\rho_{nir} - \rho_{red}}{\rho_{nir} + 6 \times \rho_{red} - 7 \times \rho_{blue} + 1} \tag{2}$$

$$NDVI = \frac{\rho_{nir} - \rho_{red}}{\rho_{nir} + \rho_{red}} \tag{3}$$

where ρ_{blue}, ρ_{green}, ρ_{red}, ρ_{nir}, and ρ_{swir} are the blue, green, red, near-infrared, and shortwave infrared bands of the Sentinel-2 and Landsat OLI imagery, respectively. We used mNDWI combined with vegetation indices (EVI and NDVI) to reduce commission errors of mixed pixels when identifying water bodies. The water body identification method used is given by Equation (4) [18,29].

$$Water = \begin{cases} 1, EVI < 0.1 \ and (mNDWI > EVI \ or \ mNDWI > NDVI) \\ 0, Other \ values \end{cases} \tag{4}$$

2.4.2. Algorithms for Patch Density (PD) and Submerged Elasticity Index (SEI)

The landscape index is a simple quantitative indicator that reflects the spatial configuration and structural composition at the landscape scale and can provide highly concentrated landscape information [35]. Landscape patch density is used to measure the degree of landscape fragmentation in a period [36,37]. Water birds are likely to inhabit areas with large expanses of open water to avoid human interference. Therefore, to some extent, we can say that the lower the patch density value of an open water body, the less suitable is that environment for water bird habitat. Open water body patch density (PD) was calculated from Equation (5):

$$PD = \frac{N}{A} \tag{5}$$

where N is the number of open water body patches where we vectorize the extracted open water surface and count the number of closed water surfaces. A is the open water body area (m²). We calculated the PD value of each lake for each month, to quantify dynamic changes and the spatial distribution of the open water body within one year.

The frequency of water bodies (F_{water}) in a year is calculated using Equation (6):

$$F_{water} = \frac{\sum N_{water}}{N_{month}} \tag{6}$$

where F_{water} is the frequency of open surface water bodies scaled between 0 and 1 among all the target images, $\sum N_{water}$ is the sum of each pixel of water bodies in one year, and N_{month} is the total number of target images in one year.

The submerged elasticity index (SEI) is an improved index based on Feng et al. [19], who defined inundation area as the area between the maximum and minimum submerged areas and we use the ratio of the inundation area to the maximum submerged area to represent the hydrological regulative capacity, calculated using Equation (7):

$$SEI = \frac{A_{max} - A_{min}}{A_{max}} \tag{7}$$

where A_{max} and A_{min} are the maximum and minimum water body area for each lake, respectively.

2.4.3. Algorithms for EVI

The satellite images were segmented into water body and non-water body (grassland, mudflat, reeds, forest, and others) [38]. Non-water bodies were the main habitats for water birds, as it provides food for them. EVI has a good fit with vegetation growth and is closely related to plant photosynthesis [39] and so we used EVI to reflect greenness of habitat and as a proxy for biomass or food abundance at the site. Equation (2) was used to extract the mean EVI value time series for non-water bodies for each lake in GEE. All the statistical analysis described here was carried out using SPSS software (IBM SPSS Statistics 19, IBM Inc., USA).

3. Results

3.1. Water Body Areas, Distribution, Variation, and Patch Densitiy (PD)

The areas and distribution of water surfaces were extracted from the multi-source remote sensing data for 2017 (Figure 3A) and 2018 (Figure 3B). It can be seen from the figures that PY and DT, which connected to the Yangtze River, have the similar hydrological regime. The largest water body areas occur in wet season (basically in July and August) and smallest water body areas occur in the dry season (from December until February). A different situation is apparent for the lakes in JH, which are isolated from the Yangtze River. In this case, the largest water surface area occurs in October, November, and December in 2017, and in November and December in 2018. There is little variation of waterbody over the course of the year for the lakes in JH.

The PD of the two types of lakes is also significantly different. DT (Figure 3C,F) and PY (Figure 3D,G) have a U-shaped trend, while the trend for the lakes in JH (Figure 3E,H) is the opposite, with an inverted U-shape in 2018. P values of all fitting results are less than 0.01, which can be seen from Figure 3. The difference between the maximum and minimum of the patch density of DT, PY, and lakes in JH was 1.97, 1.58, and 1.14 in 2017, and 1.91, 1.88, and 0.39 in 2018, respectively. The average value of the patch density for DT and PY is greater than for JH in both 2017 and 2018.

The PD indices for PY are strongly correlated with the water level data recorded at Xingzi Hydrological Station in 2017 and 2018, indicating that the PD index extracted by remote sensing does match the fluctuation of the lake water level (Figure 3I). We define dry and common years according to the data from representative Xingzi Hydrological Station in Poyang Lake over the past 60 years.

The average annual water levels of Xingzi Station is 13.31 m [40], while the average annual water level in 2018 was 11.91 m, which is classified as a dry year. The average water level in 2017 was 13.05 m, which is approached to 13.31 m, is regarded as the common year (Figure 3J). This difference can be observed by comparing the water surface maps, Figure 3A with Figure 3B.
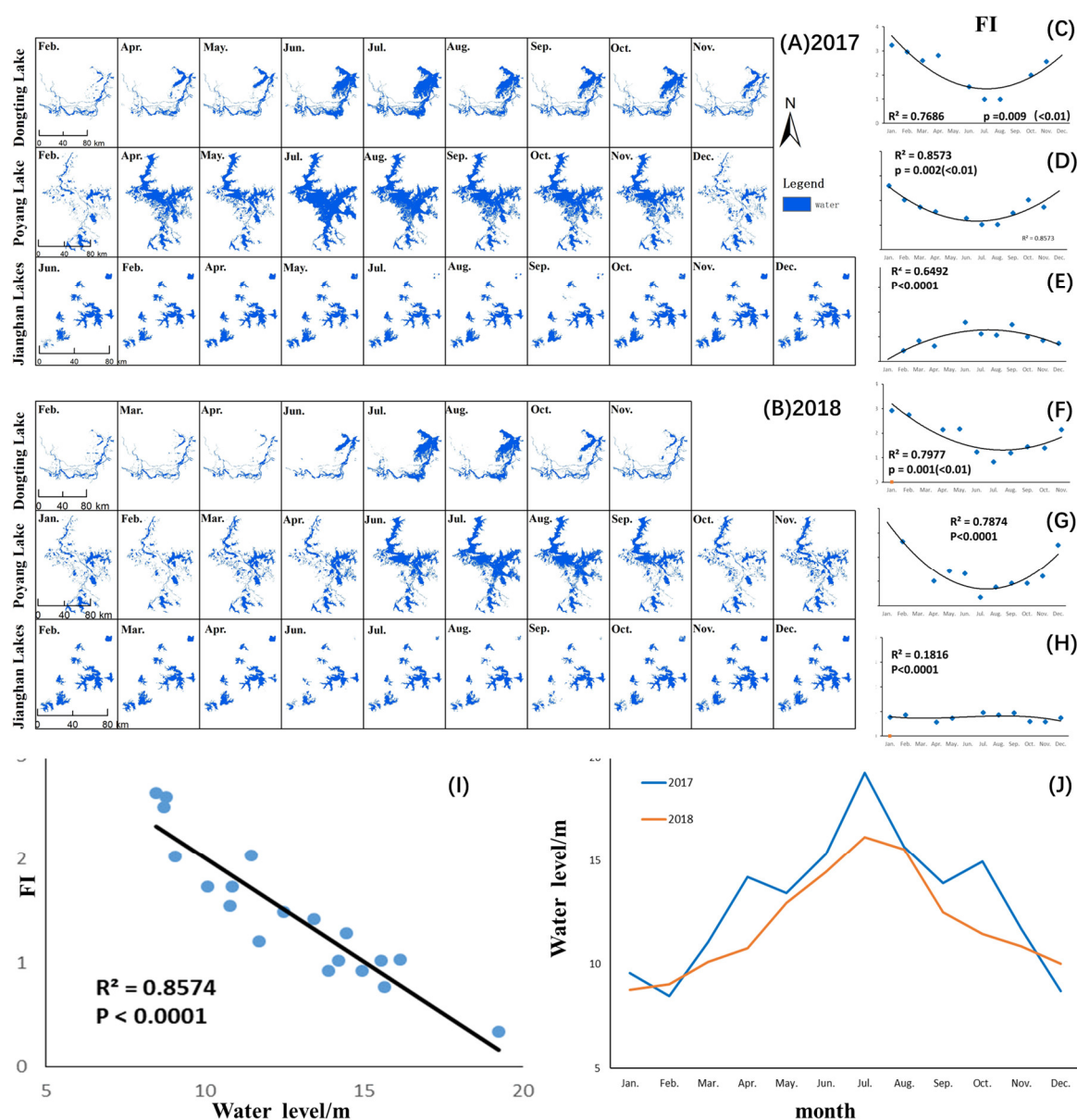

Figure 3. Water surface distribution of DT, PY, and JH extracted from remote sensing images in (**A**) 2017 and (**B**) 2018. The trend of PD in (**C**) PY, (**D**) DT, and (**E**) JH in 2017. The trend of PD in (**F**) PY, (**G**) DT, and (**H**) Jianghan Lakes in 2018. (**I**) shows the relationship between PD index and water level data from Xingzi Station in Poyang Lake. (**J**) shows the monthly average water level at the Poyang Lake Xingzi Station in 2017 and 2018.

3.2. Water Body Frequency, Trends, and Submerged Elasticity index (SEI)

The water body frequency can reflect the spatial distribution of the inundation area (Figure 4) and the submerged frequency within a year. We defined water pixels with annual water frequencies ≥75% as year-long water bodies, while the other water pixels were classified as either inundation areas (annual water frequency ≥20%) or ephemeral water bodies (<20%). For JH, in 2017 (Figure 4C) and 2018 (Figure 4E), the graph of water body frequency to total area ratio tends to rise from low to high, with year-long water bodies having the largest proportion (0.74 in 2017 and 0.90 in 2018). The

ratio of inundation area is only about 0.17 in 2017 and 0.32 in 2018. PY and DT showed different behavior.

In 2017 (Figure 4C), the water body frequency to total area ratio for DT and PY is also gradually increasing, although it increases less than in the case of the lakes in JH. The inundation area ratios in DT and PY, with values of 0.48 and 0.34, respectively, were also higher than in JH. In 2018 (Figure 4E), the year-long water body area ratio for DT and PY decreased and the inundation area increased (0.61 and 0.59). In particular, the arid part of the inundation area (water frequencies <40%) formed a large proportion of the inundation area compared to 2017.

The SEI of PY and DT is much higher than for the lakes in JH in both two years (Figure 4D). For PY and DT there is little difference in the value of SEI between 2017 and 2018, while for the lakes in JH the SEI in 2018 is almost double the 2017 value.
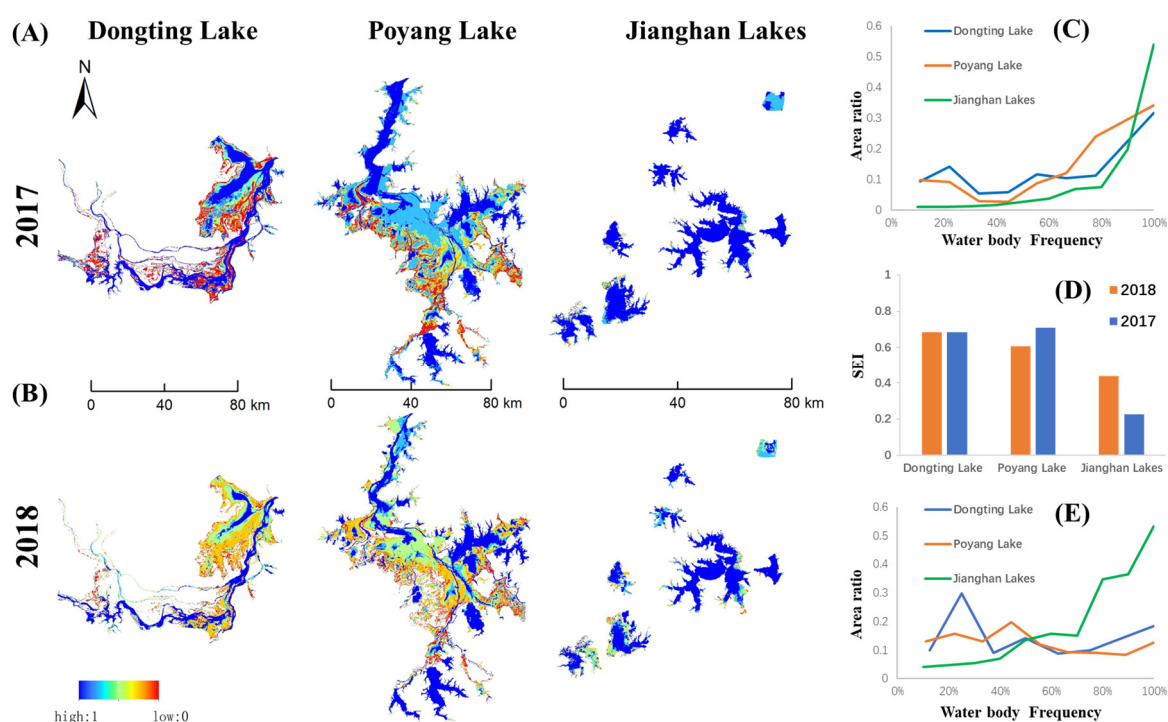

Figure 4. Water body frequency maps for DT, PY, and JH in 2017 (**A**) and 2018 (**B**). (**C**) Area ratio of water body frequencies for PY, DT, and JH in 2017 (**C**) and 2018 (**E**). (**D**) Submerged elasticity index (SEI) for DT, PY, and JH in 2017 and 2018.

3.3. Vegetation Variation and Correlation between Mean Enhanced Vegetation Index (EVI) and Pacth Desentiy (PD)

The distribution and variety of mean EVI in the three regions in 2017 (mean EVIA) and 2018 (Figure 3B) was also tested. The mean EVI of JH Lakes is lowest in winter and reaches its peak in summer in 2017 (Figure 5E) and 2018 (Figure 5H). In contrast, PY (Figure 5C) and DT (Figure 5D) reach the maximum mean EVI in winter with the smallest values occurring in summer. It is worth noting that in 2018, the mean EVI of PY (Figure 5F) and DT (Figure 5G) had two peaks, which occurred in March and April. P values of all fitting results are less than 0.0001, which can be seen from Figure 5.

We find a significant correlation between PD and mean EVI in these lakes: $p = 0.036$ ($p < 0.05$), n = 28 in 2018 (Figure 5I) and $p = 0.049$ ($p < 0.05$), n = 29 in 2017 (Figure 5J). In this study, $p < 0.05$ means that there is a statistical difference. The PD explained 15% and 20% of the variation of the mean EVI in 2018 and 2017, respectively.
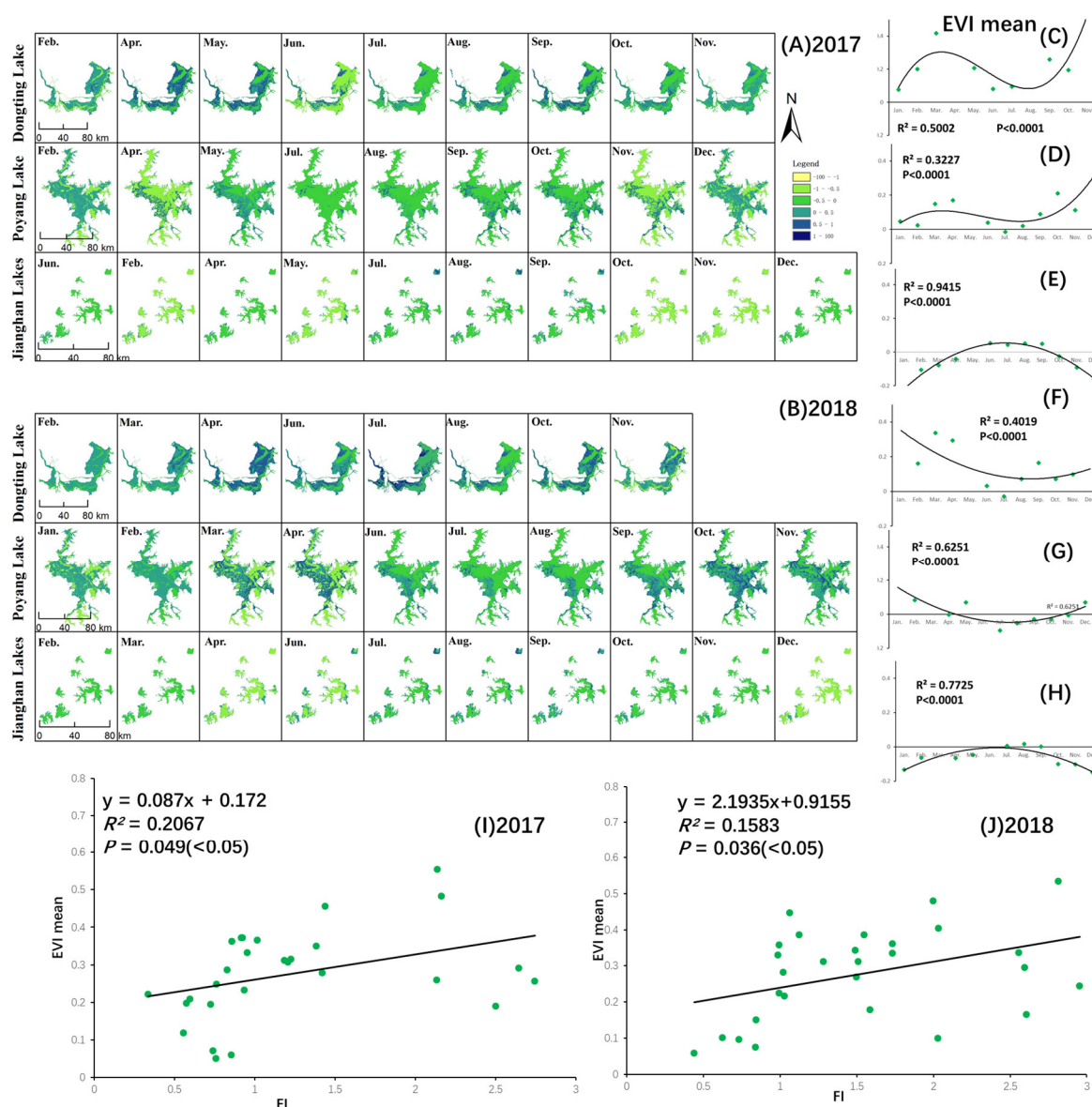
Figure 5. Annual variation of EVI for DT, PY, and JH in (**A**) 2017 and (**B**) 2018. The trend of mean EVI for (**C**) PY, (**D**) DT, and (**E**) JH in 2017. The trend of PD for (**F**) PY, (**G**) DT, and (**H**) JH in 2018. The relationships between the PD and mean EVI for DT, PY, and JH in 2017 (**I**) and 2018 (**J**).

4. Discussion

4.1. The Differences of Regulative Flexibility Between Hydrologically Connected Lakes and Isolated Lakes

Our results support that lakes with a naturally fluctuating water level have greater regulative flexibility in response to extreme environments. The main difference in the regulating capacity of connected lakes and isolated lakes lies in the extent of seasonal flooding areas. This adjustment difference leads to changes in wetland structure, such as PD, which leads to changes in wetland function. We use PD, SEI, and the inundation areas to characterize the regulative flexibility. PD can quantify the degree of fragmentation in land use type and landscape scale [35]. Whether in a drought year (2018) or an average year (2017), PY and DT exhibit higher values of PD and SEI than the values for the isolated lakes in JH, implying that the former have a stronger regulative flexibility due to effective inundation areas and greater landscape diversity. PD showed a positive correlation with size of inundation area. Moreover, PD can also reflect ecosystem structures and the larger the PD, the more separated and heterogeneous is the composition of habitat. In the wet season, when water level rises and the open water surface area expands, the PD index of PY and DT is the smallest of any time

in the year. In the dry season, as the water level drops, the mudflat and wet meadow areas become exposed [2], and PD reaches its maximum value for the year, which is beneficial for feeding migratory waterfowl [1]. However, such regular wet-dry alternation is hardly ever seen in isolated lakes. For the isolated lakes in JH, this lack of alternation is mainly because a stable water level is imposed by natural rainfall and human water consumption [8]. Year-long water bodies make up the largest proportion of JH, in both dry (2018) and wet (2017) years.

However, the area of inundation increased in 2018, due to drought in the autumn. Inundation area refers to the area that is submerged by a flood pulse and then exposed in a periodic hydrological wet-dry cycle [19]. The extent of inundation area in different lakes varies in such a periodic hydrological cycle due to lake size, hydrological traits, and the hydrological connectivity caused by human interference. Generally, it is thought that a hydrologically isolated lake will adversely affect the abundance of most creatures, because it indicates the presence of a low proportion of available habitat and have negative ecological and hydrological impacts to floodplain wetlands [41–43]. For lakes in the same floodplain, the hydrological connectivity becomes the main factor. Hydrological fluctuations bring food resources and energy exchange to the inundation area of the lake. Therefore, these areas are more effective to the ecological processes and their functions more effective than the fixed maximum water boundaries [3].

The SEI is higher in PY and DT, compared with lakes in JH. An inter-annual comparison revealed that SEI in JH doubled in the drought year of 2018 compared to 2017, while for PY and DT there is little difference in SEI values between the two years. Our study came to a similar conclusion. It shows that the naturally fluctuating lakes have better stability, flexibility, and self-regulation. The results also show that drought events can benefit isolated lake systems by increasing the hydrological cycle and easing the negative effects caused by dams.

What should be mention is that there are also limitations in this research. The influence of weather and clouds cannot avoid, and multi-sources data, such as Radar images, maybe combined in the future work to composite high-frequency data series. Besides, ground investigation data, such as soil moisture, vegetation species diversity etc., should also be considered when developed the indicators to represented physical differences of hydrological connected and isolated lakes.

4.2. Impacts of Hydrological Regimes on Habitat Availability and Quality

The hydrological regimes in connected lakes and isolated lakes are different and these differences will affect wildlife habitat availability and quality. Vegetation index, EVI, and NDVI for example, derived from remote sensing data can be used to represent the growth stage of plants, which is usually closely related to herbivore food quality [44]. These vegetation indices are widely used in the modeling of habitats for herbivores [45,46], water birds [47] or deer [48]. The vegetation index has different trends in lakes with natural fluctuations (DT and PY) and in isolated lakes.

The mean EVI for DT and PY showed a U-shaped trend which is like the trend of PD. The lowest mean EVI occurs in summer, when most vegetation is submerged, and the highest values occur in winter. In the drought year, the mean EVI showed two peak values for the connected lakes, which may be caused by the delayed rising water level in spring which, unusually, enabled the vegetation to continue growing and reach a peak around April. The mean EVI in the isolated lakes is consistent with the phenology of local vegetation growth, with a growing season from April to September. The EVI mean of JH has a lower range of variation in the whole year than PY and DT, ranging from −0.2 to 0.2. This lower range occurs because the lakes in JH have a relative stable water level and so the inundation area which favors the distribution of vegetation is small.

Connected lakes provide a higher quantity and quality of food for water birds than the isolated lakes. It also evident that the inundation areas, which favor habitat availability, correlate with water bird abundance [1]. Different birds occupy different niches in wetlands, while the wetland landscape diversity in connected lakes is higher (shown as a high PD index), and habitats are more accessible [49].

Habitat quality is mainly reflected in food resources (expressed as the EVI index). The median EVI area lasts longer, that is, the vegetation is in the early development stage, and the habitat quality

is higher [50]. Mudflat and wet meadow in the inundation areas, as well as water bodies composed wetland structure in the Yangtze River floodplain, form a natural barrier to humans, enabling aquatic animals, such as water birds, to make their habitats [1].

4.3. Management Implications for Waterbird Conservation

The open access of remote sensing data and the availability of the GEE platform offer the possibility of quick and accurate extraction of inundation areas. This work provides a case study of an effective way to gain insight into floodplain and inundation areas which will save a large amount of ground survey work. The key to improving global biodiversity conservation is to protect habitats and increase habitat availability and quality for wild animals [51]. The construction of dams leads to unprecedented uncertainty in the floodplain regimes, posing new challenges for conservation management. Predicting inundation frequencies and vegetation growth processes is necessary to obtain suitable indicators for wetland management [38].

Our research shows that lakes with natural hydrological fluctuations have a higher degree of regulatory flexibility, due to the relatively large extent of their inundation areas and greater habitat heterogeneity. The results suggest some wetland management techniques that may be effective: Enlarge inundation areas through water level manipulation [52], pump the water from isolated lakes to simulate drought status, and increase natural hydrological fluctuations in lakes through manual intervention, to meet the requirements of specific species.

5. Conclusions

This paper presents an effective method to determine the inundation areas, as well as a quantitative method to assess the impacts of hydrological connectivity on lakes. The following main conclusions are as follows:

The proportion of seasonal inundation areas is the root cause of the differences between the ecosystem structure and function of connected lakes and isolated lakes. The range of seasonal inundation areas in the former is nearly twice or three times that of the latter. Thus, it leads to higher landscape diversity and higher productivity in connected lakes than that of isolated ones, both of which are responsible for maintaining higher biodiversity.

The response of connected lake to extreme climate has higher regulation flexibility. It has a significant difference of seasonal inundated areas between drought year (in 2018) and common year (in 2017) in isolated lakes, while it is opposite in connected lakes which indicates that the ecosystems in connect lakes are more stable, in the other words, it has higher flexibility in regulation.

Different hydrological conditions resulting in different availability of habitat and the quality of habitat food. The stable water level in isolated lakes may have negative effect on biodiversity, especially on feeding of water birds. Thus, the connected lakes provide more food resources for water birds. We suggest that through hydrological regulation and interference measures, restoring the wet and dry alternation pattern and enlarge the seasonal inundation area in isolated lakes to benefit their biodiversity.

Author Contributions: This research presented here was carried out in collaboration between all authors. Conceptualization, J.T., S.X., and X.Y.; Data collection and investigation J.T., J.C. and W.S.; Methodology, J.T. and S.X.; Writing—original draft preparation, J.T.; Writing—review and editing, S.X., Y.L., P.C., H.D., and X.Y.; Supervision, X.Y.; Project administration, S.X., and X.Y.; funding acquisition, S.X., and X.Y. All authors have read and agreed to the published version of the manuscript.

Conflicts of Interest: The authors declare no conflict of interest.

References

1. Jia, Q.; Wang, X.; Zhang, Y.; Cao, L.; Fox, A.D. Drivers of waterbird communities and their declines on Yangtze River floodplain lakes. *Boil. Conserv.* **2018**, *218*, 240–246.
2. Guan, L.; Wen, L.; Feng, D.; Zhang, H.; Lei, G. Delayed Flood recession in central Yangtze floodplains can cause significant food shortages for wintering geese: Results of inundation experiment. *Environ. Manag.* **2014**, *54*, 1331–1341.
3. Lu, C.; Jia, Y.; Jing, L.; Zeng, Q.; Lei, J.; Zhang, S.; Lei, G.; Wen, L. Shifts in river-floodplain relationship reveal the impacts of river regulation: A case study of Dongting Lake in China. *J. Hydrol.* **2018**, *559*, 932–941.
4. Tockner, K.; Pusch, M.; Borchardt, D.; Lorang, M.S. Multiple stressors in coupled river-floodplain ecosystems. *Freshw. Boil.* **2010**, *55*, 135–151.
5. De Leeuw, J.; Shankman, D.; Wu, G.; De Boer, W.F.; Burnham, J.; He, Q.; Yesou, H.; Xiao, J. Strategic assessment of the magnitude and impacts of sand mining in Poyang Lake, China. *Reg. Environ. Chang.* **2009**, *10*, 95–102.
6. Riis, T.; Hawes, I. Relationships between water level fluctuations and vegetation diversity in shallow water of New Zealand lakes. *Aquat. Bot.* **2002**, *74*, 133–148.
7. Poff, N.L.; Allan, J.D.; Bain, M.B.; Karr, J.R.; Prestegaard, K.L.; Richter, B.D.; Sparks, R.E.; Stromberg, J.C. The natural flow regime. *BioScience* **1997**, *47*, 769–784.
8. Wang, J.; Sheng, Y.; Tong, T.S.D. Monitoring decadal lake dynamics across the Yangtze Basin downstream of Three Gorges Dam. *Remote Sens. Environ.* **2014**, *152*, 251–269.
9. Mei, X.; Dai, Z.; Fagherazzi, S.; Chen, J. Dramatic variations in emergent wetland area in China's largest freshwater lake, Poyang Lake. *Adv. Water Resour.* **2016**, *96*, 1–10.
10. Feng, L.; Hu, C.; Chen, X.; Zhao, X. Dramatic inundation changes of China's two largest freshwater lakes linked to the Three Gorges Dam. *Environ. Sci. Technol.* **2013**, *47*, 9628–9634.
11. Feng, L.; Han, X.; Hu, C.; Chen, X. Four decades of wetland changes of the largest freshwater lake in China: Possible linkage to the Three Gorges Dam? *Remote Sens. Environ.* **2016**, *176*, 43–55.
12. Scott, D.; Gomez-Velez, J.D.; Jones, C.N.; Harvey, J.W. Floodplain inundation spectrum across the United States. *Nat. Commun.* **2019**, *10*, 5194.
13. Hirabayashi, Y.; Mahendran, R.; Koirala, S.; Konoshima, L.; Yamazaki, D.; Watanabe, S.; Kim, H.; Kanae, S. Global flood risk under climate change. *Nat. Clim. Chang.* **2013**, *3*, 816–821.
14. Paz, A.R.; Bravo, J.M.; Allasia, D.; Collischonn, W.; Tucci, C.E.M. Large-scale hydrodynamic modeling of a complex river network and floodplains. *J. Hydrol. Eng.* **2010**, *15*, 152–165.
15. Wen, L.; Macdonald, R.; Morrison, T.; Hameed, T.; Saintilan, N.; Ling, J. From hydrodynamic to hydrological modelling: Investigating long-term hydrological regimes of key wetlands in the Macquarie Marshes, a semi-arid lowland floodplain in Australia. *J. Hydrol.* **2013**, *500*, 45–61.
16. Nakmuenwai, P.; Yamazaki, F.; Liu, W. Automated extraction of inundated areas from multi-temporal dual-polarization RADARSAT-2 images of the 2011 central Thailand flood. *Remote Sens.* **2017**, *9*, 78.
17. Plug, L.J.; Walls, C.; Scott, B.M. Tundra lake changes from 1978 to 2001 on the Tuktoyaktuk Peninsula, western Canadian Arctic. *Geophys. Res. Lett.* **2008**, *35*, doi:10.1029/2007GL032303.
18. Wang, X.; Xiao, X.; Zou, Z.; Chen, B.; Ma, J.; Dong, J.; Doughty, R.B.; Zhong, Q.; Qin, Y.; Dai, S.; et al. Tracking annual changes of coastal tidal flats in China during 1986–2016 through analyses of landsat images with google earth engine. *Remote Sens. Environ.* **2018**, doi:10.1016/j.rse.2018.11.030.
19. Feng, L.; Hu, C.; Chen, X.; Cai, X.; Tian, L.; Gan, W. Assessment of inundation changes of Poyang Lake using MODIS observations between 2000 and 2010. *Remote Sens. Environ.* **2012**, *121*, 80–92.
20. Hui, F.; Xu, B.; Huang, H.; Yu, Q.; Gong, P.; Huang, H. Modelling spatial-temporal change of Poyang Lake using multitemporal Landsat imagery. *Int. J. Remote Sens.* **2008**, *29*, 5767–5784.
21. Wang, Y.; Ma, J.; Xiao, X.; Wang, X.; Dai, S.; Zhao, B. Long-term dynamic of Poyang Lake surface water: A mapping work based on the google earth engine cloud platform. *Remote Sens.* **2019**, *11*, 313.
22. Chen, B.; Xiao, X.; Li, X.; Pan, L.; Doughty, R.; Ma, J.; Dong, J.; Qin, Y.; Zhao, B.; Wu, Z.; et al. A mangrove forest map of China in 2015: Analysis of time series Landsat 7/8 and Sentinel-1A imagery in Google Earth Engine cloud computing platform. *ISPRS J. Photogramm. Remote Sens.* **2017**, *131*, 104–120.
23. Pekel, J.-F.; Cottam, A.; Gorelick, N.; Belward, A.S. High-resolution mapping of global surface water and its long-term changes. *Nature* **2016**, *540*, 418–422.

24. Song, C.; Ke, L.; Pan, H.; Zhan, S.; Liu, K.; Ma, R. Long-term surface water changes and driving cause in Xiong'an, China: From dense Landsat time series images and synthetic analysis. *Sci. Bull.* **2018**, *63*, 708–716.

25. Chen, B.; Dong, J.; Qin, Y.; Xie, G.; Xiao, X.; Ye, H.; Ma, J.; Doughty, R.; Li, X.; Zhao, B.; et al. Mapping forest and their spatial-temporal changes from 2007 to 2015 in Tropical Hainan Island by Integrating ALOS/ALOS-2 L-Band SAR and landsat optical images. *IEEE J. Sel. Top. Appl. Earth Obs. Remote Sens.* **2018**, *11*, 852–867.

26. Dong, J.; Xiao, X.; Menarguez, M.A.; Zhang, G.; Qin, Y.; Thau, D.; Biradar, C.; Moore, B. Mapping paddy rice planting area in northeastern Asia with Landsat 8 images, phenology-based algorithm and Google Earth Engine. *Remote Sens. Environ.* **2016**, *185*, 142–154.

27. Zhang, W.; Li, X.; Yu, L.; Si, Y. Multi-scale habitat selection by two declining East Asian waterfowl species at their core spring stopover area. *Ecol. Indic.* **2018**, *87*, 127–135.

28. Zou, Z.; Dong, J.; Menarguez, M.A.; Xiao, X.; Qin, Y.; Doughty, R.; Hooker, K.V.; Hambright, K.D. Continued decrease of open surface water body area in Oklahoma during 1984–2015. *Sci. Total Environ.* **2017**, *595*, 451–460.

29. Zou, Z.; Xiao, X.; Dong, J.; Qin, Y.; Doughty, R.; Menarguez, M.A.; Zhang, G.; Wang, J. Divergent trends of open-surface water body area in the contiguous United States from 1984 to 2016. *Proc. Natl. Acad. Sci. USA* **2018**, *115*, 3810–3815.

30. Fox, A.D.; Cao, L.; Zhang, Y.; Barter, M.; Zhao, M.J.; Meng, F.J.; Wang, S.L. Declines in the tuber-feeding waterbird guild at Shengjin Lake National Nature Reserve, China—A barometer of submerged macrophyte collapse. *Aquat. Conserv. Mar. Freshw. Ecosyst.* **2010**, *21*, 82–91.

31. Li, C.; Li, H.; Zhang, Y.; Zha, D.; Zhao, B.; Yang, S.; Zhang, B.; De Boer, W.F. Predicting hydrological impacts of the Yangtze-to-Huaihe Water Diversion Project on habitat availability for wintering waterbirds at Caizi Lake. *J. Environ. Manag.* **2019**, *249*, 109251.

32. Wu, Z.; He, H.; Cai, Y.; Zhang, L.; Chen, Y. Spatial distribution of chlorophyll a and its relationship with the environment during summer in Lake Poyang: A Yangtze-connected lake. *Hydrobiologia* **2014**, *732*, 61–70.

33. Ye, X.; Meng, Y.; Xu, L.; Xu, C. Net primary productivity dynamics and associated hydrological driving factors in the floodplain wetland of China's largest freshwater lake. *Sci. Total Environ.* **2019**, *659*, 302–313.

34. Sheng, L.; Zhang, X.; Xu, X. Remote sensing based analysis and dynamic monitoring on area and storage of Poyang Lake. *Water Resour. Hydropower Eng.* **2010**, *11*, 84–90.

35. Ewers, R.M.; Didham, R.K. Confounding factors in the detection of species responses to habitat fragmentation. *Boil. Rev.* **2005**, *81*, 117.

36. O'Neill, R.V.; Krummel, J.R.; Gardner, R.H.; Sugihara, G.; Jackson, B.; DeAngelis, D.L.; Milne, B.T.; Turner, M.G.; Zygmunt, B.; Christensen, S.W.; et al. Indices of landscape pattern. *Landsc. Ecol.* **1988**, *1*, 153–162.

37. Hein, S.; Pfenning, B.; Hovestadt, T.; Poethke, H.-J. Patch density, movement pattern, and realised dispersal distances in a patch-matrix landscape—A simulation study. *Ecol. Model.* **2004**, *174*, 411–420.

38. Aharon-Rotman, Y.; McEvoy, J.; Zhaoju, Z.; Yu, H.; Wang, X.; Si, Y.; Xu, Z.; Yuan, Z.; Jeong, W.; Cao, L.; et al. Water level affects availability of optimal feeding habitats for threatened migratory waterbirds. *Ecol. Evol.* **2017**, *7*, 10440–10450.

39. Shi, L.; Jia, Y.; Zuo, A.; Ma, T.; Lei, J.; Zhou, Y.; Wen, L. Dynamic change of vegetation cover and productivity of Poyang Lake wetland based on MODIS EVI time series. *Biodivers. Sci.* **2018**, *26*, 828–837.

40. Dai, X.; Wan, R.; Yang, G.; Wang, X. Temporal Variation of Hydrological Rhythm in Poyang Lake and the Associated Water Exchange with the Changjiang River. *Sci. Geogr. Sin.* **2014**, *34*, 1487–1496.

41. Kingsford, R.T. Ecological impacts of dams, water diversions and river management on floodplain wetlands in Australia. *Aust. Ecol.* **2000**, *25*, 109–127.

42. Paracuellos, M. How can habitat selection affect the use of a wetland complex by waterbirds? *Biodivers. Conserv.* **2006**, *15*, 4569–4582.

43. Cumming, G.S.; Paxton, M.; King, J.; Beuster, H. Foraging guild membership explains variation in waterbird responses to the hydrological regime of an arid-region flood-pulse river in Namibia. *Freshw. Boil.* **2012**, *57*, 1202–1213.

44. Huete, A.; Didan, K.; Miura, T.; Rodriguez, E.; Gao, X.; Ferreira, L. Overview of the radiometric and biophysical performance of the MODIS vegetation indices. *Remote Sens. Environ.* **2002**, *83*, 195–213.

45. Gustine, D.D.; Parker, K.L.; Lay, R.J.; Gillingham, M.P.; Heard, D.C. Calf survival of woodland caribou in a multi-predator ecosystem. *Wildl. Monogr.* **2006**, *165*, 1–32.

46. Wiegand, T.; Naves, J.; Garbulsky, M.; Fernández, N. Animal habitat quality and ecosystem functioning: Exploring seasonal patterns using NDVI. *Ecol. Monogr.* **2008**, *78*, 87–103.

47. Roshier, D.; Asmus, M.; Klaassen, M. What drives long-distance movements in the nomadic Grey Teal Anas gracilis in Australia? *IBIS* **2008**, *150*, 474–484.

48. Showers, S.E.; Tolleson, D.R.; Stuth, J.W.; Kroll, J.C.; Koerth, B.H. Predicting diet quality of white-tailed deer via NIRS fecal profiling. *Rangelands* **2006**, *59*, 300–07.

49. Xu, Y.; Si, Y.; Yin, S.; Zhang, W.; Grishchenko, M.; Prins, H.H.T.; Gong, P.; De Boer, W.F. Species-dependent effects of habitat degradation in relation to seasonal distribution of migratory waterfowl in the East Asian-Australasian flyway. *Landsc. Ecol.* **2019**, *34*, 243–257.

50. Wei, J.; Xin, Q.; Ji, L.; Gong, P.; Si, Y. A new satellite-based indicator to identify spatiotemporal foraging areas for herbivorous waterfowl. *Ecol. Indic.* **2019**, *99*, 83–90.

51. Cao, L.; Zhang, Y.; Barter, M.; Lei, G. Anatidae in eastern China during the non-breeding season: Geographical distributions and protection status. *Boil. Conserv.* **2010**, *143*, 650–659.

52. Coops, H.; Beklioglu, M.; Crisman, T.L. The role of water-level fluctuations in shallow lake ecosystems—Workshop conclusions. *Hydrobiologia* **2003**, *506*, 23–27.